University of Zaragoza

Master in Physics and Physical Technologies

Correlation of thermoelectric and spin properties in magnetic oxides

Author:
Alberto
Anadón Barcelona

Supervisors:
Dra. Myriam H. Aguirre
Dr. Rafael Ramos Amigo

June 23, 2013

Universidad Zaragoza

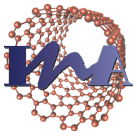

Instituto Universitario de Investigación en Nanociencia de Aragón
Universidad Zaragoza

Contents

Abstract

Thermoelectrics are a potentially transformative power generation technology because they possess the property to convert directly heat into an electric voltage. In addition, thermoelectrics are a pollution-free method for generating energy. Until last decade, efficiency of thermoelectric materials has remained low, but due to the study of nanostructured materials they are becoming promising for commercial use. In this work we will be introduced in the world of thermoelectric characterization. For this purpose we are going to perform thermal, transport, thermoelectric and magnetic measurements in bulk single crystal magnetite and polycrystalline bismuth.

1 Introduction

Power generation of renewable energy is one of the most important challenges for science and technology. Fossil fuel combustion is an inefficient way of generating energy, since only 25 % of the generated energy is usable [6]. The remaining 75 % is lost by different mechanisms: radiation and friction (5 %); exhaust gas (40 %) and dissipation in the engine (30 %). One way to exploit this wasted energy is the use of thermoelectric (TE) devices. Previously, TE materials were used mainly in concrete applications (see figure 1), but in order to improve waste-heat recovery technologies, TE devices are becoming more prominent.

The origin of thermoelectricity dates back to 1822 when the Seebeck Effect[23] (SE) was discovered giving rise to devices such as thermocouples, very extended for measuring temperature nowadays. SE consist of a voltage difference that appears within any conducting material that is subjected to a temperature gradient $\Delta V = S\Delta T$ showing a proportional relation, where S is the Seebeck coefficient. Twelve years after, Jean Peltier discovered the reverse effect[18]. He found that the passage of an electric current (I) through a thermocouple produces a small heating or cooling depending on its direction

$$q = \pi I, \tag{1}$$

where q and π are the heat flux and Peltier coefficient, respectively.

In 1851, W. Thomson predicted theoretically (and observed experimentally) when a thermal gradient and an electrical current are induced to a conductor whose S magnitude is variable with temperature, a heating or cooling process is produced, due to the S variation[10]. The evolution of the heat flow can be described by equation 2.

$$\dot{q} = -\tau \mathbf{J} \cdot \nabla T, \tag{2}$$

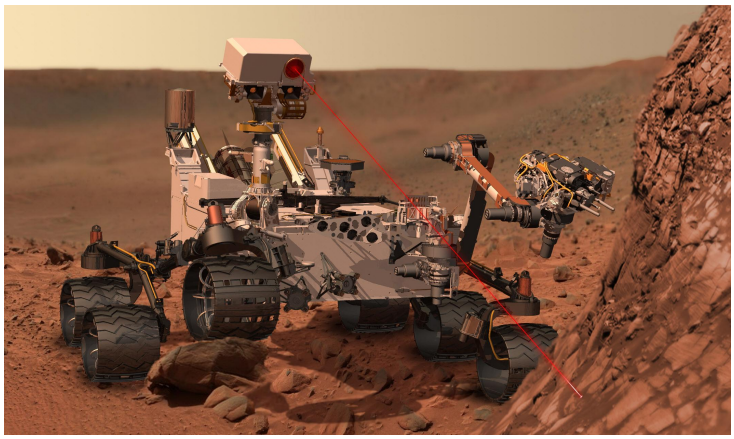

Figure 1: Robotic rover Curiosity is powered by a radioisotope TE generator. Radioisotope power systems are generators that produce electricity from the decay of radioactive isotopes. Heat given off by the decay of this isotope is converted into electricity by a TE system, providing constant power for fourteen years, the lifetime of the isotope used. *Autor and copyright: NASA*

where $\dot{q}$, τ, $\mathbf{J}$ are the heat flow per second, Thomson coefficient and current density though a homogeneus conductor. Thomson also related and summarized all the three effects in the following relations (1854)[1]:

$$\tau = T\frac{dS}{dT} \tag{3}$$

$$\pi = ST \tag{4}$$

Today's thermoelectrics aim at increasing the heat to electricity conversion efficiency. The TE efficiency in power generation mode is defined in equation 5[6], and is limited by the Carnot efficiency, $\epsilon_C = \frac{T_H - T_C}{T_H}$. TE efficiency in power generation mode is calculated as the ratio of the electrical energy extracted from the source to the quantity of heat applied[10].

$$\epsilon = \epsilon_C \frac{\sqrt{1+ZT_M}-1}{\sqrt{1+ZT_M}+T_C/T_H}, \tag{5}$$

Where T_H, T_C and T_M are the hot, cold and average temperatures respectively. An important magnitude to obtain the efficiency of a TE material is the figure of merit $ZT = \frac{S^2\sigma T}{\kappa}$, where σ represents the electrical conductivity, T the absolute temperature and κ the thermal conductivity. We will define these quantities more precisely in section 2.

For real applications it is desirable to have a figure of merit greater than one for the efficiency to be large enough. In literature, a ZT higher than

two[28] has been estimated for p and n type TE materials by reduction of the thermal conductivity through heat transport control in nanostructured devices. Another novel approach to achieve higher thermoelectric efficiency is the study of thermoelectric effects in magnetic materials such as the Nernst Effect (NE)[30] or the recently discovered Spin Seebeck Effect (SSE)[26][20], which have already shown potential for possible applications[27].

Classic thermoelectric materials are usually semiconductor alloys, as we will see later. Most of the materials used are Bi_2Te_3 and Sb_2Te_3 alloys, since they have the greatest ZT value for n- and p-type bulk materials at room temperature.

In this work we propose to study thermoelectric and thermomagnetic phenomena in Bismuth and Magnetite.

Bismuth is a semimetal with one of the lowest thermal conductivity observed for metals (7.97 W/mK at room temperature). An image of a bismuth crystal can be seen in figure 2a. It was the material used by Nernst and Ettingshausen in the discovery of the Nernst effect[8] (NE). Bismuth has also the largest NE coefficient[2] observed for correlated metals due to exceptionally low value of carrier density and also due to a very long electronic mean-free path in clean single crystals. Bismuth is also the most naturally diamagnetic material and when it is deposited in thin films with a thickness comparable to its Fermi wavelength a transition to semiconductor occurs due to electron confinement.

Magnetite is known since ancient Greece to attract metals. An image of a magnetite crystal can be seen in figure 2b. It is the strongest natural permanent magnet (ferrimagnetic material) with a Curie temperature of 858 K. It is an iron oxide (Fe_3O_4) with inverse spinel structure (cubic) and formula $A^{2+}B_2^{3+}O_4^{2-}$. The oxygen anions are arranged in a face centered cubic lattice and the A and B cations occupy 1/8 of the tetrahedral and 1/2 of the octahedral interstices respectively. In magnetite the A sites are occupied by half of the Fe^{3+} ions, while the B sites are occupied by equal number of Fe^{2+} and Fe^{3+} ions arranged in rows along the <110> directions (the double exchange between these ions is the main reason for magnetite being an electric conductor at room temperature). Magnetite also presents a metal to insulator transition at around 125 K called the Verwey transition.

(a) (b)

Figure 2: Bismuth crystals (a) and magnetite crystal (b).

2 Thermoelectrics

2.1 Seebeck and Peltier effects

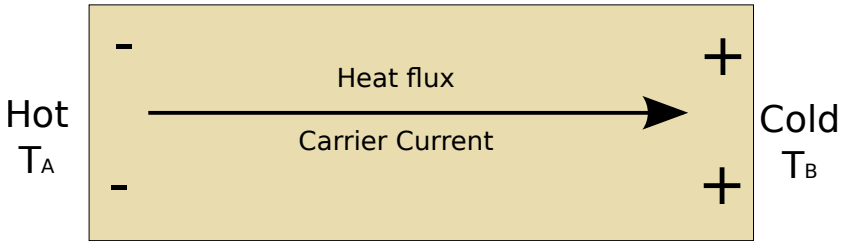

Figure 3: Detail of the Seebeck effect configuration. Plus and minus sign represent the relative electric potential sign with respect to the centre if dominant carriers are electrons.

An electrical voltage difference (ΔV) appears within any conducting material that is subjected to a temperature gradient; this is called the Seebeck effect[23], and was discovered by the Baltic German physicist Thomas Johann Seebeck in 1822. Seebeck saw that a compass needle was deflected when a temperature gradient was applied on two different metals connected in a closed loop. He did not understood the SE in the terms it is interpreted nowadays, but rather as a magnetic effect, so he called the phenomenon the thermomagnetic effect. Later on, it was discovered by Hans Christian Ørsted that the deflection was caused by a magnetic field generated by an electrical current in the loop, discarding the magnetic nature of the effect.

SE is due to carrier diffusion from the hot to the cold sides[5]. Figure 3 shows a diagram of SE. The Seebeck coeficient, S, is defined as the instantaneous rate of change of the SE with respect to temperature (eq. 6) at a constant temperature.

$$S = \left(\frac{dV}{dT}\right)_T \tag{6}$$

If S is independent from temperature, equation 6 can be written as:

$$\Delta V = S\Delta T \tag{7}$$

Where ΔT is the temperature difference between the hot and cold sides. In SI the Seebeck coefficient is usually expressed in $\mu V/K$.

The inverse effect was discovered by French physicist Jean Charles Athanase Peltier in 1834. When a voltage difference is applied to a conducting material, a thermal gradient may appear in it. As T.J. Seebeck, Peltier saw the effect by applying a current (I) to a loop with two different conducting materials. In the junction between them heat was absorbed or generated depending on the current direction. This is the working principle of the thermopile (see figure 4). The heat flux in a Peltier junction between two conducting materials A and B is given by equation 8

$$q = (S_A T_A - S_B T_B)I \tag{8}$$

2.2 Thermal conductivity

The thermal conductivity (κ) is the coefficient that relates heat flux (heat flowing through unit area every second) and temperature gradient for isotropic materials, as it is written in equation 9. Its units are W/mK in SI.

$$\mathbf{q} = \kappa \nabla T \tag{9}$$

From equation 5 and the definition of ZT in section 1, it is deduced that, to increase the TE efficiency in power generation mode (this is also valid for TE efficiency in refrigeration mode[6]), we need to reduce κ as much as possible without compromising the value of electrical conductivity and Seebeck coefficient. Thermoelectric devices also require low thermal conductivity materials to reduce the transfer of heat across each leg. Because of this, in TE materials it is important to distinguish between electronic (κ_e) and lattice (κ_l) thermal conductivity. The sum of the different conductivities is the total thermal conductivity defined in equation 9. There also exist other systems, such as aerogels or thermal barrier coatings in wich we need

to consider other kind of carriers[25], but, for simplicity, here we consider electrons and phonons as carriers.

$$\kappa = \kappa_e + \kappa_l \tag{10}$$

In modern TE materials, the improvement of ZT is usually achieved by minimizing the value of κ_l[31], since κ_e is directly related with the electrical conductivity by the empirical Wiedemann-Franz law:

$$\kappa_e = L\sigma T, \tag{11}$$

Where $L = \frac{\pi^2}{3}\left(\frac{k_B}{e}\right)^2 = 2.44 \cdot 10^{-8}\ W\Omega K^{-2}$ is the Lorenz factor.

After a huge effort in experimental research, it was discovered that alloying semiconductors with high carrier concentration increases the efficiency of bulk thermoelectric materials, because they have high carrier concentration, which gives them a good and tuneable electrical conductivity. Besides, the transport of phonons is disrupted due to the different atomic elements involved, reducing their thermal conductivity.

2.3 Thermopiles and thermocouples

Termopiles consist on many couples of n-type (negative S) and p-type (positive S) thermoelectric legs wired electrically in series and thermally in parallel (See figure 4). The configuration is similar for thermocouples, in which two wires of p and n materials are soldered together in one edge and a voltage difference is measured at the other. The opposite S sign in each leg of the thermopile and the serial connections between the p-n couples maximize the voltage difference across the output electrical connections.

2.4 Figure of merit

As it was defined in section 1 the figure of merit is given by:

$$ZT = \frac{S^2\sigma T}{\kappa} \tag{12}$$

It is always positive and TE efficiency becomes larger as the value of ZT increases (see figure 5).

There are mainly two aproaches to obtain high ZT in addition to minimizing lattice thermal conductivity, one of them is the fabrication of nanoestructured devices[6][15]. They can enhance the density of states near Fermi level because of quantum confinement and therefore increase the Seebeck coefficient, which becomes decoupled from the electrical conductivity.

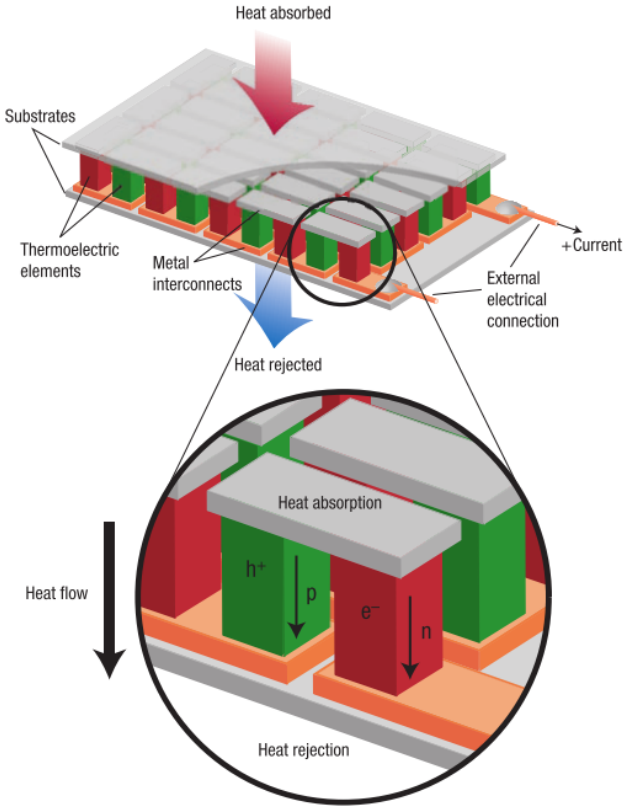

Figure 4: Detail of a thermopile[24].

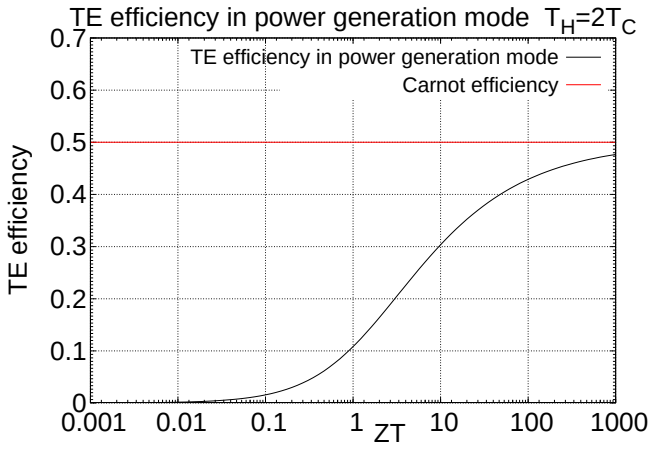

Figure 5: TE efficiency in power generation mode for $T_H = 2T_C$.

The other is the the *phonon glass electron crystal* approach, which suggests that an ideal thermoelectric material should be the combination of glass-like thermal conductivity and crystal-like electronic properties[21].

2.5 Nernst Ettingshausen effect

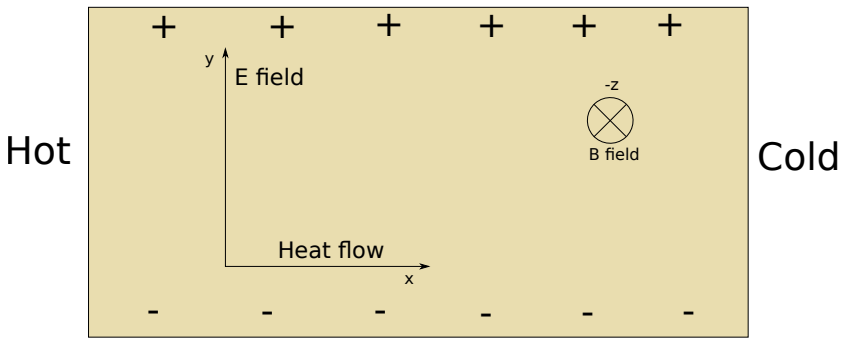

Figure 6: Detail of the Nernst configuration.

When a magnetic field (**B**, in z direction) is applied to a conducting material subjected to a thermal gradient (∇T, in the x direction), besides the previously described effects, a transversal voltage difference (electric field $\mathbf{E_{NE}}$, in y direction) appears due to the Lorentz force[7]. A graphical representation of NE is shown in figure 6. The definition of Nernst coefficient (N) is given in equation 13. N is usually expressed in $\mu V/KT$.

$$\mathbf{E_{NE}} = N\mathbf{B} \times \nabla T \rightarrow N = \frac{dV/dy}{B_z dT/dx} \tag{13}$$

For an isotropic material and considering that N does not change with temperature, we can write that:

$$N = \frac{\Delta V}{B\Delta T}\frac{\Delta x}{\Delta y} \tag{14}$$

The Ettingshausen and Nernst effects are related to each other in the same way as the Peltier and Seebeck effects. The Ettingshausen effect is a transverse temperature gradient perpendicular to an electric current that is the result of a magnetic field transversal to both of them. The Ettingshausen coefficient (P) is defined by the following equation[10]:

$$P = NT/\kappa \tag{15}$$

From these effects new possibilities emerge. We can now define the thermomagnetic figure of merit as[10]:

$$ZT_{NE} = \frac{(NB_z)^2 \sigma T}{\kappa} \tag{16}$$

2.6 Anomalous Nernst effect

In 1879 Edwin H. Hall[11] discovered the so called "Hall effect", when a current is flowing in a conductor and it is subjected to a magnetic field, the Lorentz force deviates its electrons against one side of the conductor. Some years later, he discovered that for iron, the effect was ten times larger[12]. This is today known as the anomalous Hall effect (AHE)[17]. The regular HE presents a Hall resistivity (ρ_{xy}) linear with the applied magnetic field with coefficient R_0 and it is explained by considering Lorentz force acting on a constant current. In the case of the AHE, the Hall resistivity is not linear, but it depends empirically on the magnetization (M_z) of the sample as follows[17]:

$$\rho_{xy} = R_0 H_z + R_s M_z \tag{17}$$

Unlike R_0, which was already understood to depend mainly on the density of carriers, R_s is not completely understood.

For ferromagnetic materials it is found that the Nernst coefficient is connected to Hall resistivity by the Mott relation[30][19].

Empirically, it is found that anomalous Nernst effect (ANE) is a phenomenon that generates an electric voltage in the cross product direction between the magnetization and temperature gradient in ferromagnetic materials[22, 16]:

$$\mathbf{E_{ANE}} = \mu_0 Q_S (\mathbf{M} \times \nabla T), \tag{18}$$

Where μ_0 and Q_S are vacuum permeability and anomalous Nernst coefficient, respectively.

3 Experimental techniques

3.1 Magnetic characterization

Magnetic characterization of samples was realized on a Magnetic Properties Measurement System (MPMS) fabricated by Quantum Design. The

Figure 7: MPMS (left) and PPMS (right) used in the samples characterization.

equipment belongs to the physical measurements service of the University of Zaragoza. A photograph of the equipment is shown in figure 7 (left).

An SQUID (from Superconducting Quantum Interference Device) sensor is used to measure the magnetization of samples. It is based on superconducting loops containing Josephson junctions[9]. The flux variation inside the loop is converted to an electric current by tunnelling across the junctions.

The system is able to perform measurements from 1.9K to 400K applying a maximum magnetic field of 50 kOe.

It has two different measurement modes: DC and RSO. The first mode is slower and less sensitive (from 5×10^{-9} *emu* without applying magnetic field to 10^{-4} at maximum field applied). The second mode is able to detect about 10^{-7} *emu* without applying magnetic field and 2×10^{-7} at maximum field applied. In this mode, sensibility is improved by moving the sample sinusoidally though the SQUID coils.

3.2 Thermal transport measurements

3.2.1 Seebeck effect and Thermal conductivity measurements

Seebeck effect and thermal conductivity measurements were performed by a PPMS-9T (from Physical Properties Measurement System) and PPMS-14T, both of them fabricated by Quantum Design. A photograph of the equipment is shown in figure 7 (right). This equipment is able to measure Seebeck

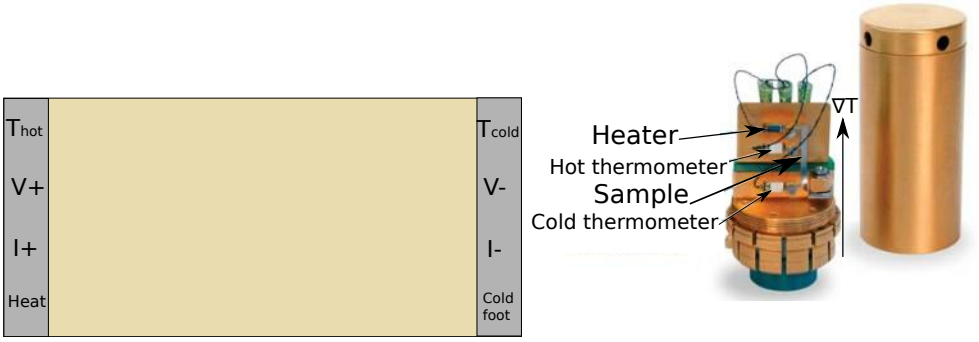

Figure 8: Two-probe scheme for Seebeck effect and thermal conductivity measurements (left) and photograph of the thermal transport puck with radiation shield (right).

and thermal conductivity from 1.9 K to 400 K applying a maximum magnetic field of 14 T (9 T for the PPMS-9T) with the thermal transport option (TTO) of PPMS. In TTO mode, the system measures thermal conductivity by monitoring the temperature drop along the sample while a known amount of heat passes through the it. To avoid radiation and convection losses, the sample is encapsulated using a radiation shield and kept in high vacuum (about 10^{-4} mbar). It is also able to measure the Seebeck effect as an electrical voltage drop between V_+ and V_- (see figure 8).

Two measurement modes are available: continuous and single measurement mode. In both of them a pulse of heat is introduced into the system and the response is studied. To do that, temperature is monitored in both thermometers: T_{cold} and T_{hot} (see figure 8). Voltage drop is also measured between V_+ and V_-. The system is also able to perform electrical conductivity measurements in this mode by applying an electric current between I_+ and I_- and measuring the voltage difference between V_+ and V_-. This is not done at the same tame, since the heat pulse could affect the measurement result, but after the system is stable. In the continuous mode, measurements are being taken continually and the software is adjusting parameters (such as heater power) to optimize the measurements. It is faster than single mode, but also less sensitive. In single mode the system reaches a steady state in both the initial and end states, so the values are not calculated but measured directly.

3.2.2 Electrical conductivity measurements

In addition to PPMS, a different system was used for electrical conductivity measurements and also for thermoelectric measurements. The equipment

was developed in the Institute of Nanoscience of Aragón (INA). It consist of a series of devices connected among themselves and controlled by a computer. They are:

- Keithley 2821a nanovoltmeter. Low noise measurements at high speeds in the nV scale.
- Keithley 236 source meter to control injected current from 100 fA to 100 mA
- Keithley 2000 6 1/2 digits multimeter with an input impedance higher of 10 GΩ
- Continuous flux Oxford instruments cryostat. It allows us to measure from 4 K to 400 K.
- HV-4V series electromagnet. It is able to reach a magnetic field of 1 T powered by a TDK-Lambda source.

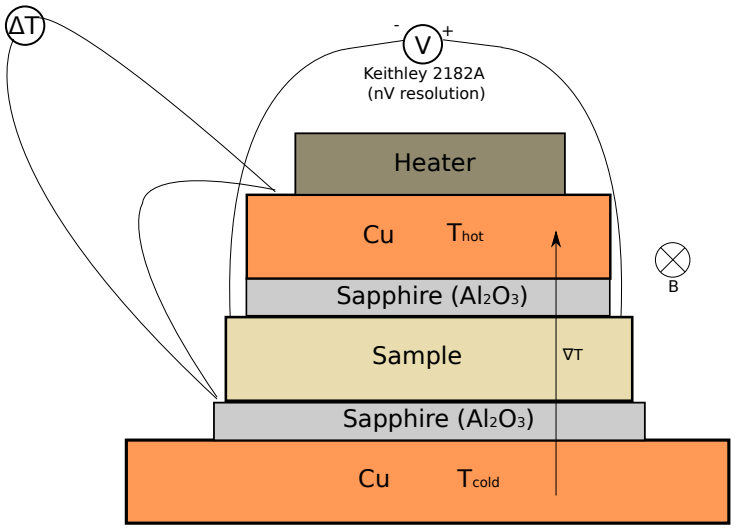

Figure 9: Set-up configuration for NE measurements.

3.2.3 Nernst effect measurements

For Nernst effect measurements an attoLIQUID cryogenic system fabricated by attocube systems was used in addition to the Oxford instruments cryostat system described in the previous section. It is a liquid Helium bath cryostat with 50 l cryogenic liquid reservoir. It has been optimized for high stability

and low-noise for magnetic microscopy and modified for transport measurements. It has a base temperature of 4.2 K which can be reduced down to 1.8 K by pumping on the Helium reservoir. Temperature is controlled via a variable temperature insert down to mK scale with a PID (or feedback) software. Two superconducting electromagnets are included in both z axis (8 T) and y axis directions (2 T). This feature allows the application of a 3D vectorial magnetic field by rotating the sample.

In addition, we developed a PC controlled system that consists on:

- Keithley 2821a nanovoltmeter. Low noise measurements at high speeds in the nV scale.
- Keithley 2635 source meter with a dynamic range from 1 fA to 10 A in current and 1 μV to 200 V in voltage mode. Used for applying a highly stable current to the heater.
- Keithley 2000 6 1/2 digits multimeter. Used for measuring the temperature drop across the sample with two T-type thermocouples connected differentially.

In the sample holder set-up the sample is electrically insulated from the copper pieces by two sapphire single crystals, as it is show in figure 9. Sapphire, being an insulator, has a high thermal conductivity (about 35 W/mK at room temperature (RT), and higher at lower temperatures[3]). Copper presents one of the highest thermal conductivities (about 400 W/mK at RT), which is a crucial feature for achieving fast thermal stability. Temperature drop in the sample is measured between top copper part and bottom sapphire piece by two thermocouples. Both copper parts are attached by two Teflon screws (See figure 10), that have low thermal conductivity (about 0.25 W/mK at RT). 3D CAD software was used for the design of both set-ups. They are shown in figure 10.

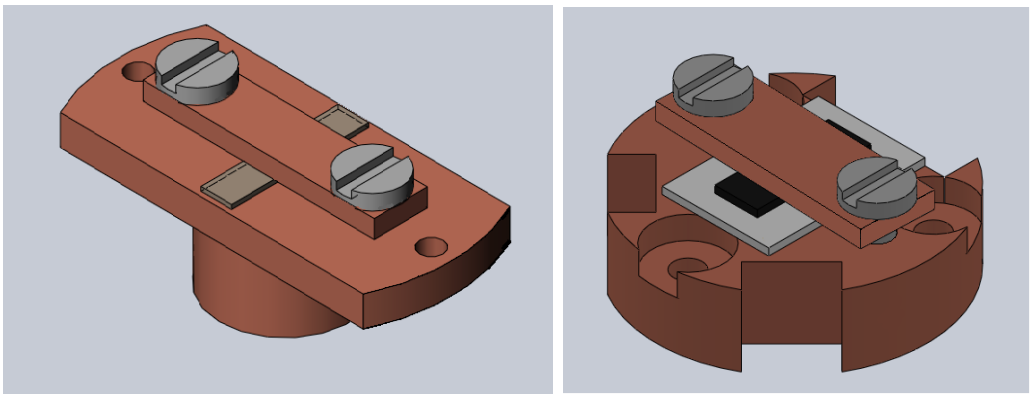

Figure 10: 3D CAD image of the set-up described in figure 9. It was fabricated at the INA for NE measurements in the attocube systems cryostat (left) and in the Oxford instruments cryostat (right). Acknowledgement R. Ramos.

4 Results

4.1 Bismuth

Samples of 99.999 % pure polycrystalline bismuth were used in order to calibrate the Nernst effect measurement set-up (see fig. 9). Previous to the Nernst effect measurements, the samples were characterized using the TTO mode in the PPMS (described in section 3.2.1) to check with previous experiments reported in the literature[13, 7]. As it was described, TTO mode allows us to perform thermal transport (Seebeck coefficient and thermal conductivity) and electrical transport measurements at the same time. Thermal and electrical conductivity measurements are represented in figure 11. Electrical conductivity shows a typical metallic behaviour, with a resistivity of 2.70(2) $\mu\Omega$m at 300 K. Electrical conductivity for polycrystalline bismuth is barely constant because it is dominated by scattering at the grain boundaries, since it is much less than the mean free path of carriers[4]. Heat in Bi at low temperature is essentially carried by phonons because of the low electrical carrier concentration. At low temperatures, thermal conductivity decreases because heat capacity of a crystal and thermal conductivity, wich is proportional to heat capacity, tends to vanish when temperature tends to zero. When the temperature increases, the electronic contribution increases.

Seebeck effect measurements are in perfect agreement with previously reported values[4] as can be seen in figure 12.

Once the quality of the samples was checked, the calibration of Nernst coefficient in our set-up was started. Initial measurements were made using

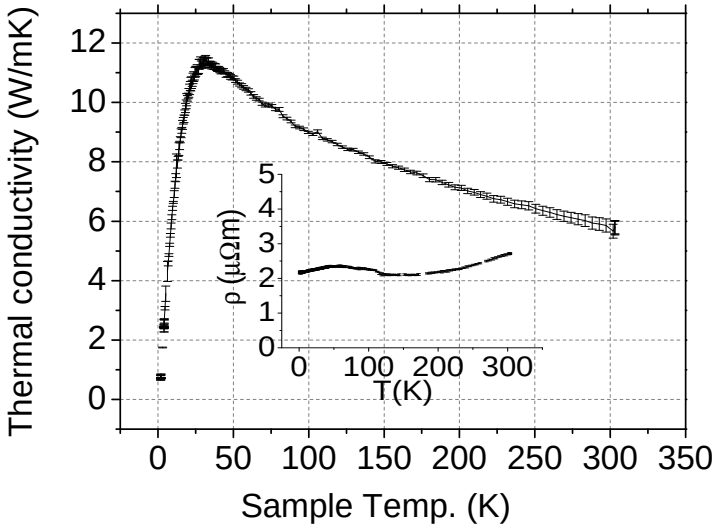

Figure 11: Thermal conductivity and electrical resistivity of a polycrystalline Bi sample measured with TTO mode of the PPMS.

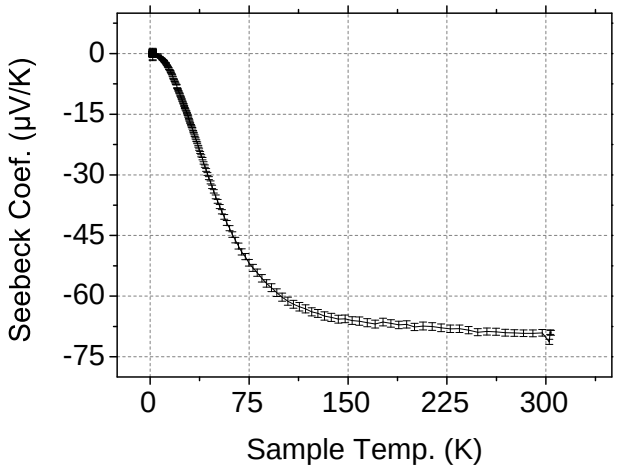

Figure 12: Seebeck coefficient of a polycrystalline Bi sample measured with TTO mode of the PPMS.

kapton tape as the electrical insulator (with thickness 130 μm and 30 μm). The obtained coefficients were smaller than expected because the measured gradient between copper plates is an overstimation of the real gradient across the sample (due to low thermal conductivity of kapton). In order to correct this problem we used sapphire single crystal as the electrical insulator ma-

terial, whose thermal conductivity is about 35 W/mK at RT and increases significantly at decreasing temperatures[3].

Nernst coefficient was calculated for each temperature, considering the slope obtained from the dependence of the voltage measured in the y direction with the applied magnetic field ($Vy(H)$). This is done for different gradients as shown in figure 13, exhibiting a linear dependence. From the dependence of the slope of $Vy(H)$ for different ΔT, we can extract the Nernst coefficient (equation 14) for the polycrystalline Bismuth, obtaining the values shown in table 1. This values are in perfect agreement with the ones previously reported by Hamabe et al[13] at 200 K and 300 K.

Temperature	Hamabe et al. 2003[13]	Our results
200K	-100.5(1) μV/K	-99(2) μV/KT
300K	-17.8(4) μV/K	-16(1) μV/KT

Table 1: Nernst coefficient values comparison for 200 K and 300 K.

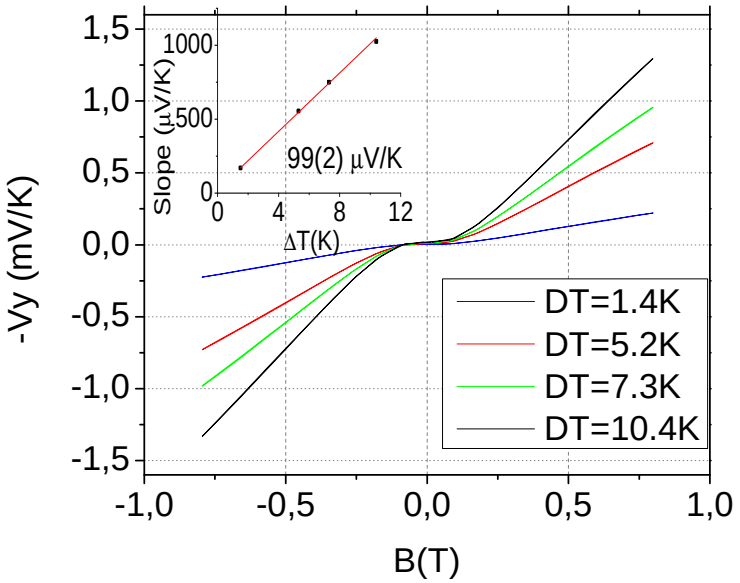

Figure 13: Nernst coefficient of a polycrystalline Bi sample at 200 K measured in the Oxford instruments cryostat system for different thermal gradients.

4.2 Magnetite

A magnetite single crystal sample was used to measure thermal conductivity in the same set-up as bismuth samples. The result can be seen in figure 14. Thermal conductivity is approximately constant at temperatures higher than the Verwey transition. This behaviour is a similar to what has been previously observed in metals[25]. Below the Verwey transition it follows a typical insulator behaviour[25].

Additionally, electrical resistivity of a magnetite single crystal sample was measured in PPMS using regular resistivity mode. Figure 15 shows both the resistivity and magnetization dependence on temperature for the magnetite single crystal. As seen in figure 15, the sample presents the Verwey transition at 123 K. This is a clear indication of the good stoichiometry of our sample[14]. Theoretically, there are two different approaches to explain electrical conductivity behaviour in magnetite[29]: Mott's model and Ihle–Lorenz's model. Mott's model explains the Verwey transition as a phase change from a Winger glass ($T > T_V$) to a Winger crystal ($T < T_v$) and describes more adequately the low-temperature behaviour. Ihle–Lorenz's model assumes a a superposition of polaron-band and hopping conductivity and is in better agreement with the measurements at high temperature.

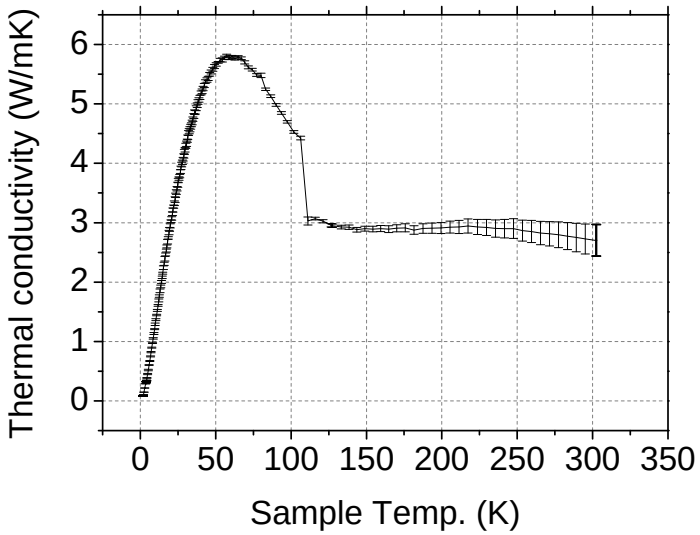

Figure 14: Thermal conductivity of a magnetite single crystal sample measured with TTO mode of the PPMS.

Seebeck effect measurements were also performed and are consistent with those found in the literature[14] (figure 16). We have obtained a sign reversal

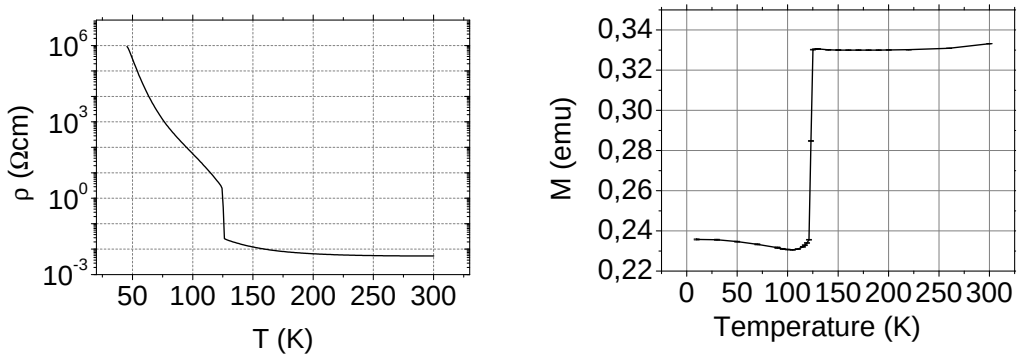

Figure 15: Electrical resistivity (left) and magnetization (right) of a magnetite single crystal sample. Resistivity was measured with PPMS and magnetization was measured with the MPMS.

and an enhanced Seebeck effect below the Verwey transition, with a peak at a temperature close to the peak in the thermal conductivity. This might be due to the phonon drag and it has also been previously observed. At temperatures below 50 K the sample resistivity (figure 15) increases significantly and Seebeck signal is out of the range of detection of PPMS.

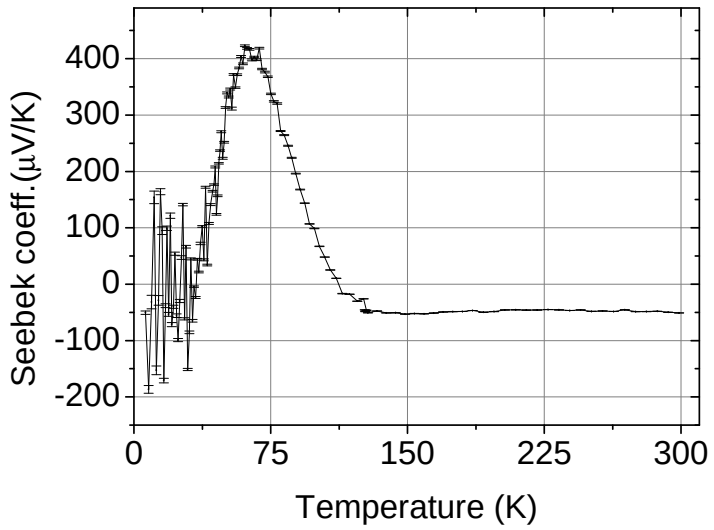

Figure 16: Seebeck coefficient of a magnetite single crystal sample measured with TTO mode of the PPMS.

Nernst coefficient measurements were performed at the attocube cryostat system. The behaviour presented by magnetite is different from that of

bismuth. Figure 17 shows a measurement of the Nernst effect at a sample temperature of 150 K and an applied thermal gradient of $T = 5\ K$. It is interesting to note that the measured voltage follows the same behaviour with the applied magnetic field as the magnetization of the sample. This effect is called the anomalous Nernst effect and is the thermoelectric analogue of the anomalous Hall effect in magnetic materials.

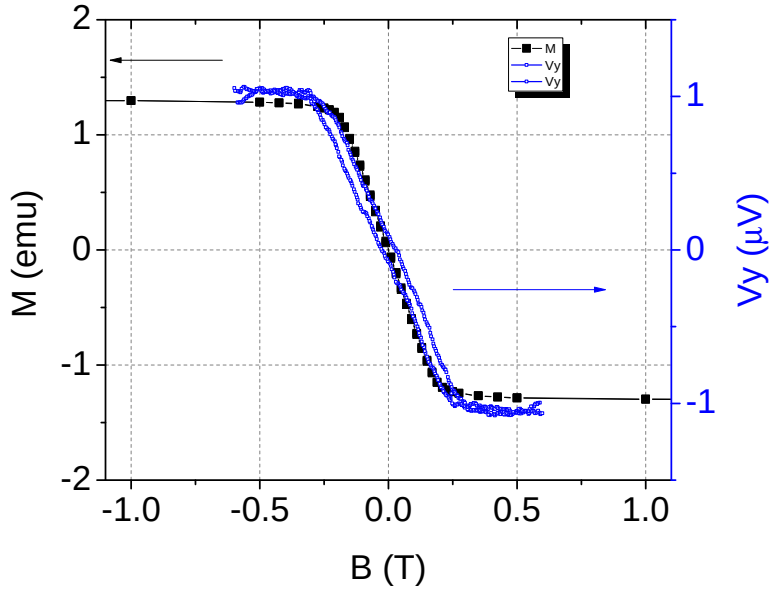

Figure 17: Sample magnetization for a magnetite single crystal at 140 K and $\Delta T = 5$ K. It is found to be proportional to Nernst coefficient, as it happens in AHE.

The temperature dependence of the anomalous Nernst effect field (E_{ANE}) normalized with the applied thermal gradient is represented in figure 18. The voltage difference ΔV represented in figure 18 corresponds to half the difference between saturated voltages at negative and positive magnetic field ($\Delta V = (V(+H) + V(-H))/2$). At temperatures lower than the Verwey transition (T_V) the ANE could not be measured. This can be due to a change of the conduction behaviour below the Verwey transition, wich yields an increased resistivity and reduced number of charge carriers[29]. The Seebeck effect (symmetric part with the magnetic field) dominates the observed signal below T_V. Further systematic measurements of the magneto-Seebeck effect are required in order to fully understand this result.

Saturation values for Nernst voltage scales linearly with the thermal gradient, as can be seen in figure 19 and as it was expected from equation 18.

Sample was rotated in YZ plane (see figure 6) and it was found that the anomalous Nernst effect is negligible when the magnetic field is applied in the direction parallel to the voltage drop, in agreement with equation 18. This can be seen in figure 20.

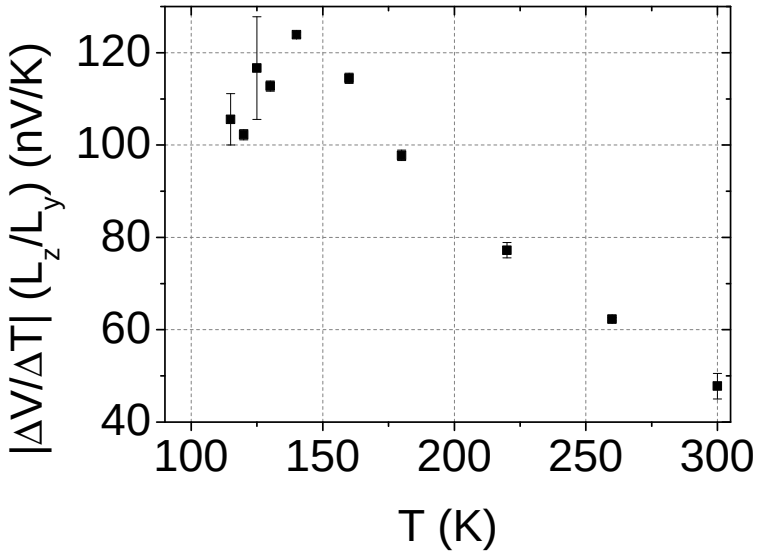

Figure 18: Anomalous Nernst effect dependence with temperature. ΔV represents half the difference between saturated voltages at negative and positive magnetic field.

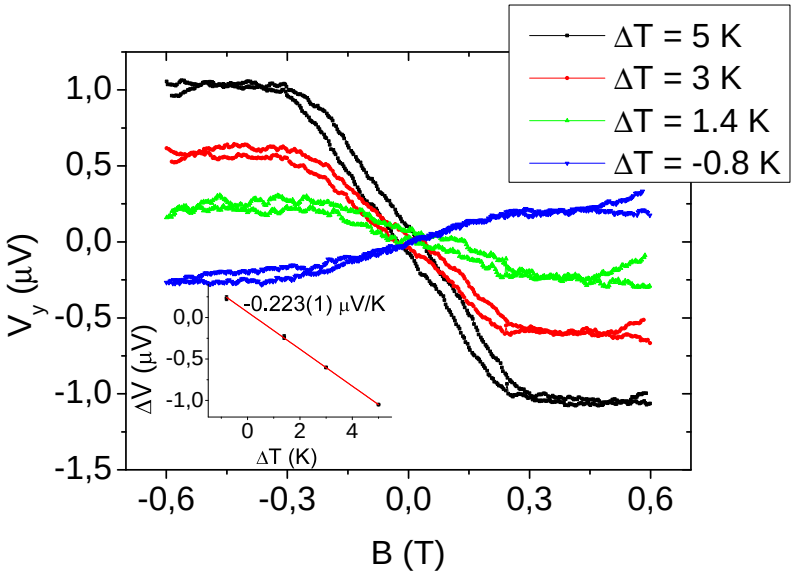

Figure 19: Nernst coefficient dependence with thermal gradient at 140 K. We can see that the voltage difference has got a linear dependence with the applied thermal gradient.

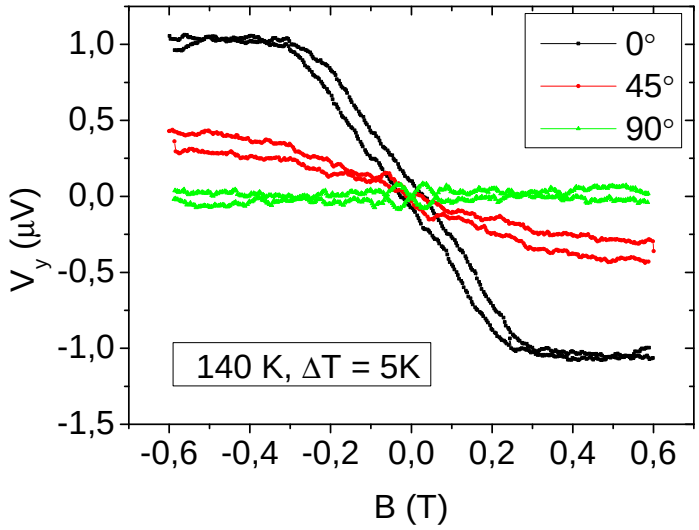

Figure 20: Angular dependence of Nernst coefficient at 140 K.

5 Conclusions

Thermoelectric measurements were performed on a polycrystalline bismuth sample with a purity of 99.999%. The obtained resistivity, Seebek and thermal conductivity values were within expectation. After the quality of samples was confirmed we performed Nernst effect measurements on the polycrystalline bismuth to calibrate our experimental set-up. A value of 16(1) μV/KT at 300 K was obtained, in perfect agreement with the values previously reported[13].

Magnetite single crystal samples were also characterized by thermal transport, electrical transport and magnetization measurements. Verwey transition was observed at 123 K by conductivity and magnetization measurements. This is a clear indication of the good stoichiometry of our sample. Electrical conduction in magnetite is usually explained in terms of a superposition between electron hopping and polaron-band conductivity. Seebek effect measurements present a peak at a temperature close to the peak in the thermal conductivity. Considering the low carrier density at temperatures below the Verwey transition, this might be due to the phonon drag. It has been found that the magnetite single crystal samples present the anomalous Nernst effect because the observed Nernst voltage was proportional to magnetization. It has also been checked that anomalous Nernst effect in the samples follows the expected behaviour (see equation 18) when thermal gradient and orientation with respect to applied magnetic field was changed.

Anomalous Nernst effect is a barely unexplored phenomenon both experimentally and theoretically. It might lead to better performance in thermoelectric generation and refrigeration[22], one of the pollution-free methods that are being investigated in order to generate energy and improve waste-heat recovery technologies.

References

[1] L. I. Anatychuk and O. J. Luste. Generalized thermoelectric thomson relations. In *Thermoelectrics, 2003 Twenty-Second International Conference on - ICT*, pages 491–492, 2003. http://ieeexplore.ieee.org/xpls/abs_all.jsp?arnumber=1287555.

[2] Kamran Behnia, Marie-Aude Méasson, and Yakov Kopelevich. Nernst Effect in Semimetals: The Effective Mass and the Figure of Merit. *Physical Review Letters*, 98(7):076603, February 2007. http://link.aps.org/doi/10.1103/PhysRevLett.98.076603.

[3] R. Berman, E. L. Foster, and J. M. Ziman. Thermal Conduction in Artificial Sapphire Crystals at Low Temperatures. I. Nearly Perfect Crystals. *Proceedings of the Royal Society A: Mathematical, Physical and Engineering Sciences*, 231(1184):130–144, July 1955. http://rspa.royalsocietypublishing.org/cgi/doi/10.1098/rspa.1955.0161.

[4] F. Brochin, B. Lenoir, X. Devaux, R. Martin-Lopez, and H. Scherrer. Preparation and transport properties of polycrystalline Bi and Bi–SiO2 nanocomposites. *Journal of Applied Physics*, 88(6):3269, 2000. http://link.aip.org/link/JAPIAU/v88/i6/p3269/s1&Agg=doi.

[5] Herbert B. Callen. *Thermodynamics and an introduction to thermostatistics.* John Wiley & sons, 1985.

[6] Zhi-Gang Chen, Guang Han, Lei Yang, Lina Cheng, and Jin Zou. Nanostructured thermoelectric materials: Current research and future challenge. *Progress in Natural Science: Materials International*, 22(6):535–549, December 2012. http://linkinghub.elsevier.com/retrieve/pii/S1002007112001384.

[7] JCG de Sande and JM Guerra. Nernst-Ettingshausen effect in polycrystalline bismuth at high temperature. *Physical Review B*, 45(20):469–473, 1992. http://prb.aps.org/abstract/PRB/v45/i20/p11469_1.

[8] A.V. Ettingshausen and W. Nernst. *Wied. Ann.*, (29):343, 1886.

[9] D. Gignoux and M. Schlenker. *Magnetism. Vol. 2, Materials and Applications.* Springer, 2005.

[10] H. Julian Goldsmid. *Introduction to Thermoelectricity.* Springer, 2009. http://www.springer.com/materials/book/978-3-642-00715-6.

[11] E. H. Hall. *Amer. J. Math.*, 2:287, 1879.

[12] E. H. Hall. *Phil. Mag.*, 12:157, 1881.

[13] M Hamabe and S Yamamoto. Magnetic field effect for improvement of thermoelectric conversion: a proposal for Nernst-Seebeck element. *Conference on-ICT*, pages 567–570, 2003. http://ieeexplore.ieee.org/xpls/abs_all.jsp?arnumber=1287576.

[14] AJM Kuipers and VAM Brabers. Thermoelectric properties of magnetite at the Verwey transition. *Physical Review B*, 1976. http://adsabs.harvard.edu/abs/1976PhRvB..14.1401K.

[15] A. J. Minnich, M. S. Dresselhaus, Z. F. Ren, and G. Chen. Bulk nanostructured thermoelectric materials: current research and future prospects. *Energy & Environmental Science*, 2(5):466, 2009. http://xlink.rsc.org/?DOI=b822664b.

[16] Masaki Mizuguchi, Satoko Ohata, Ken-ichi Uchida Eiji, and Saitoh Koki. Anomalous Nernst Effect in an L10-Ordered Epitaxial FePt Thin Film. 5:4–6, 2012.

[17] Naoto Nagaosa, Jairo Sinova, Shigeki Onoda, A. H. MacDonald, and N P Ong. Anomalous Hall effect. April 2009. http://arxiv.org/abs/0904.4154.

[18] J. C. A. Peltier. *Ann. Chem.*, (LVI):371–387, 1834.

[19] Yong Pu, Daichi Chiba, Fumihiro Matsukura, Hideo Ohno, and Jing Shi. Mott relation for anomalous hall and nernst effects in $ga_{1-x}mn_xAs$ ferromagnetic semiconductors. *Phys. Rev. Lett.*, 101:117208, Sep 2008. http://link.aps.org/doi/10.1103/PhysRevLett.101.117208.

[20] R. Ramos, T. Kikkawa, K. Uchida, H. Adachi, I. Lucas, M. H. Aguirre, P. Algarabel, L. Morellon, S. Maekawa, E. Saitoh, and M. R. Ibarra. Observation of the spin Seebeck effect in epitaxial Fe3O4 thin films. *Applied Physics Letters*, 102(7):072413, 2013. http://link.aip.org/link/APPLAB/v102/i7/p072413/s1&Agg=doi.

[21] D. M. Rowe et al. *CRC Handbook of thermoelectrics*. CRC Press LLC, 1995.

[22] Yuya Sakuraba, Kota Hasegawa, Masaki Mizuguchi, Takahide Kubota, Shigemi Mizukami, Terunobu Miyazaki, and Koki Takanashi. Anomalous Nernst Effect in L10-FePt/MnGa Thermopiles for New Thermoelectric Applications. 6:1–4, 2013.

[23] T. J. Seebeck. Magnetische Polarisation der Metalle und Erzedurch Temperatur-Differenz. *Abhand Deut. Akad. Wiss. Berlin*, (7):265–373, 1822.

[24] G Jeffrey Snyder and Eric S Toberer. Complex thermoelectric materials. *Nature materials*, 7(2):105–14, February 2008. http://www.ncbi.nlm.nih.gov/pubmed/18219332.

[25] Eric S. Toberer, Lauryn L. Baranowski, and Chris Dames. Advances in Thermal Conductivity. *Annual Review of Materials Research*, 42(1):179–209, August 2012. http://www.annualreviews.org/doi/abs/10.1146/annurev-matsci-070511-155040.

[26] K Uchida, S Takahashi, K Harii, J Ieda, W Koshibae, K Ando, S Maekawa, and E Saitoh. Observation of the spin Seebeck effect. *Nature*, 455(7214):778–81, October 2008. http://www.ncbi.nlm.nih.gov/pubmed/18843364.

[27] Ken-ichi Uchida, Tatsumi Nonaka, Tatsuro Yoshino, Takashi Kikkawa, Daisuke Kikuchi, and Eiji Saitoh. Enhancement of Spin-Seebeck Voltage by Spin-Hall Thermopile. *Applied Physics Express*, 5(9):093001, August 2012. http://apex.jsap.jp/link?APEX/5/093001/.

[28] R Venkatasubramanian, E Siivola, T Colpitts, and B O'Quinn. Thin-film thermoelectric devices with high room-temperature figures of merit. *Nature*, 413(6856):597–602, October 2001. http://www.ncbi.nlm.nih.gov/pubmed/11595940.

[29] F Walz. The Verwey transition-a topical review. *Journal of Physics: Condensed Matter*, 285, 2002. http://iopscience.iop.org/0953-8984/14/12/203.

[30] Di Xiao, Yugui Yao, Zhong Fang, and Qian Niu. Berry-Phase Effect in Anomalous Thermoelectric Transport. *Physical Review Letters*, 97(2):026603, July 2006. http://link.aps.org/doi/10.1103/PhysRevLett.97.026603.

[31] M. Zebarjadi, K. Esfarjani, M. S. Dresselhaus, Z. F. Ren, and G. Chen. Perspectives on thermoelectrics: from fundamentals to device applications. *Energy & Environmental Science*, 5(1):5147, 2012. `http://xlink.rsc.org/?DOI=c1ee02497c`.